Ultraviolet and Visible Lasers

M. L. BHAUMIK
Northrop Corporation, Northrop Research and Technology Center
Palos Verdes Peninsula, California 90274, U.S.A.

ABSTRACT

Recently discovered excimer lasers promise for the first time the availability of high average power coherent sources in the ultraviolet and visible region of the spectrum. Significant progress has been made already by the achievement of single pulse energy as high as 30 J/liter in small lasers using e-beam as well as e-beam sustained discharge excitation. A single pulse energy of 350 J from a 60 liter e-beam excited laser has also been reported. However, in scaling these lasers to high average powers, challenging fluid dynamic problems will be encountered due to the high gas density and short laser wavelength. These problems include achieving a density perturbation ($\Delta\rho/\rho$) as low as 10^{-4} in free stream turbulence and acoustic damping of nearly 60 dB. Solutions to these crucial problems are essential to realize the full potential of the new ultraviolet and visible lasers.

INTRODUCTION

Many important applications requiring visible and shorter wavelength lasers have not been possible due to a distinct lack of efficient, high power lasers in this spectral region. Recently some significant advances have been made which promise to change this situation. The discovery of rare gas excimer and rare gas transfer lasers has provided, for the first time, most efficient and powerful sources of radiation in the uv region. This is primarily due to the fact that electrical energy can be deposited very efficiently into the rare gas excited states by e-beam or discharge pumping.

The first lasers of this type were the pure rare gas excimers [1] such as Xe_2^*. The efficiency of these lasers, however, appears to be limited by processes like photoionization and also by the lack of low-loss mirrors. Attempts were then made to utilize the efficient energy deposition in rare gases by subsequent energy transfer to a desirable laser molecule. These efforts led to the Ar-N_2 lasers [2]. Ultimately, the most efficient rare gas-based lasers have turned out to be the rare gas halide lasers where, instead of energy transfer, the excited rare gas atom undergoes a chemical reaction with the halogens, much like the alkali halides, to form an excimer.

The possibility of using rare gas halide excimers for lasers was suggested by Velazco and Setser [3]. The first rare gas halide lasers were XeF [4, 5] (350 nm), XeCl [6] (308 nm), and XeBr [7, 8] (282 nm). Shortly after the discovery of the xenon halide lasers, the Ar-I_2 (342 nm) transfer laser [9, 10] was reported. Subsequent laser experiments with other rare gas halides resulted in the development of the KrF [6, 11] laser, which is still unsurpassed by any other uv laser in energy output and efficiency. Therefore, much of the discussion will be based on the KrF laser.

All the rare gas halide excimers that have shown laser oscillations are shown in Table 1 along with their output wavelengths. These wavelengths may be shifted by stimulated Raman scattering using various gases to provide efficient coherent radiation covering a large part of the uv visible spectral region.

Table 1. Observed Emission From Rare Gas Monohalides

Peak Wavelengths in Nanometers

	He	Ne	Ar	Kr	Xe
F	(Ionic State	Fluorescence (107)	Laser (193)	Laser (248)	Laser $\binom{351}{353}$
Cl	Not Lowest		Laser (170)	Laser (222)	Laser (308)
Br	Excited		Weak Emission (166) (Predissociated?)	Fluorescence (206)	Laser (282)
I	State; apparently predissociates)			Weak Emission (185) (Predissociated?)	Fluorescence (252)

Significant advances toward this goal have been made [12] by Raman shifting of ArF and KrF lasers with efficiencies over 50%. Recent success with the mercury monohalide lasers [13] may also provide additional visible lasers. Thus the availability of efficient single pulse lasers in the uv visible region appears to be very promising indeed. However, repetitively pulsed operation of these lasers to provide high average powers poses many challenging problems. One of the most difficult problems is associated with the fluid dynamics of pulsed lasers at short wavelengths and high gas densities. A summary of these problems is presented after a state-of-the-art discussion of the KrF laser.

KRYPTON FLUORIDE EXCIMER LASER CHARACTERISTICS

Excimers are molecules that normally do not exist. They are formed only in excited states when at least one of the constituent atoms is brought to an excited state. Therefore they are represented by a bound upper state and a repulsive or weakly bound ground state. This property of the excimers makes them almost ideal candidates for high power lasers. Even though the laser transition terminates in the ground state resulting in a high quantum efficiency, there is no bottlenecking as the molecule self-destructs. The advantages of an excimer laser are further illustrated with KrF as an example.

The molecular potential energy diagram [14] for KrF is shown in Figure 1.

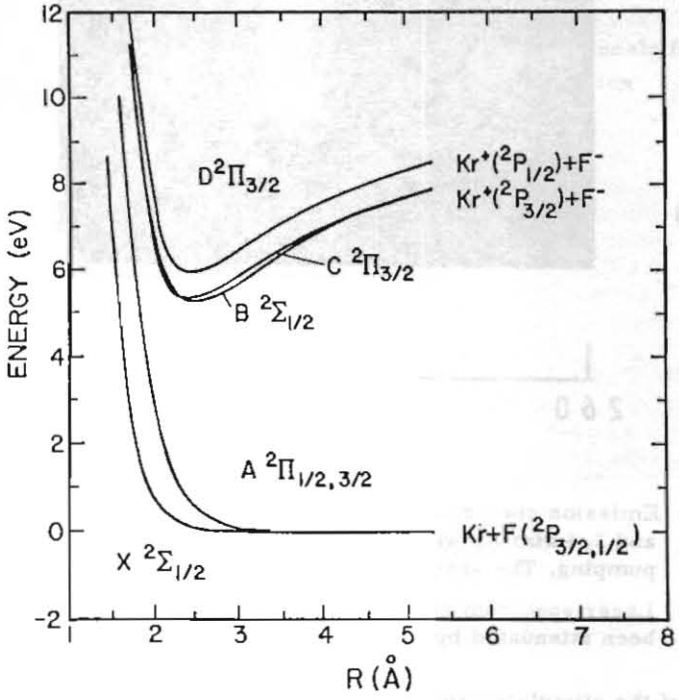

Figure 1. Potential Energy Curves for KrF

The ground state manifold arising out of covalent bonding of Kr ($^1S_0$) and F ($^2P_{3/2,\,1/2}$) consists of two branches, $^2\Sigma$ and $^2\Pi$. The $^2\Sigma$ branch has the lowest energy and is designated as the X state. The transition terminates to the nearly flat part of this curve resulting in a narrower linewidth and a higher stimulated emission cross section. On the other hand, transitions to the A $^2\Pi$ states terminate to the highly repulsive part of the curve, giving rise to a broadband emission which does not show laser oscillations.

The lowest upper states of the KrF molecule arise out of ionic bonding of Kr^+ ($^2P_{3/2,\,1/2}$) and F^- (^1S) ions. The potential of these states follows a Coulomb curve which at large internuclear distances, crosses the covalent curves corresponding to Kr^* and F atoms. Thus the excited molecules relax to the lowest ionic state irrespective of whether it is formed via the ionic or the neutral channel. The structure of the ionic upper state manifold is similar to that of the ground state manifold, with the B $^2\Sigma$ state being the lowest. The laser emission corresponds to the B ($^2\Sigma$) → X ($^2\Sigma$) transition, although a strong D → X and weak C → A transition are observed in emission.

The fluorescence due to the B - X transition is shown in Figure 2. The diffuse nature of the fluorescence is characteristic of the bound-free transition. The spectrally narrowed laser emission is also shown in Figure 2.

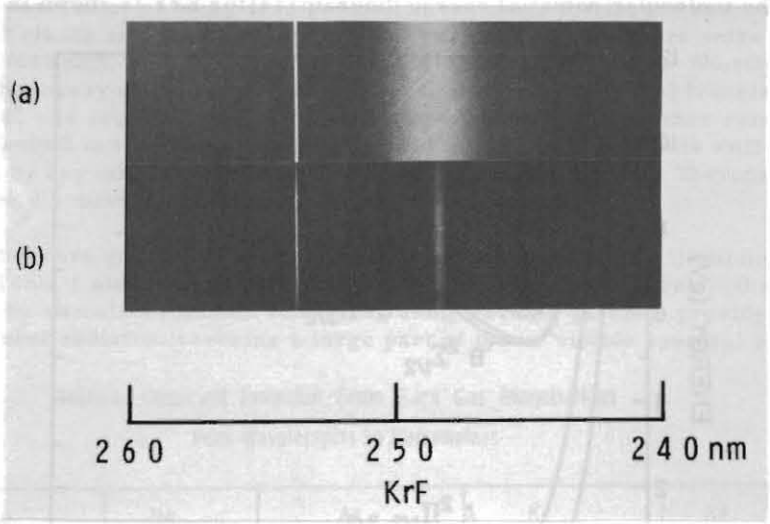

Figure 2. (a) Emission spectrum of KrF from a mixture of 2 Torr NF_3 and 3.4 atm Ar with 10% Kr obtained by electron beam pumping. The sharp line to the left is the Hg calibration line.

(b) Laser spectrum of the same mixture. The intensity has been attenuated by a factor of 10^4 to prevent film saturation.

The product of the stimulated emission cross section and the radiative lifetime of this transition has been estimated [15] to be 17 $Å^2$-ns. The lifetime of the KrF molecule has been measured [16] to be 9 ns, giving a value for the stimulated emission cross section σ for KrF of $\sim 2 \times 10^{-16}$ cm^2. This high stimulated emission cross section coupled with a dissociative ground state helps to counteract severe quenching problems of the KrF molecule and increases laser efficiency. The quenching is worst when KrF is made directly in a mixture of Kr and F_2. For this reason, a diluent such as Ar is used to minimize this problem.

KrF Formation Kinetics

The reaction kinetics for the formation of KrF^* is very complicated, although it contains only three initial species: Ar, Kr, and F_2. The important reactions and their contributions to the overall efficiency of forming KrF^* are illustrated in Figures 3 and 4 for a mixture of 2167 Torr of Ar with 110 Torr Kr and 4 Torr F_2.

The principal channels under moderate e-beam pumping proceed through the argon ion and metastable states. At current densities less than 50 A/cm^2 the principal neutralization process is ion-ion recombination (Figure 3), i.e.

$$X^+ + F^- + M \rightarrow XF + M$$
$$X_2^+ + F^- \rightarrow XF + X$$

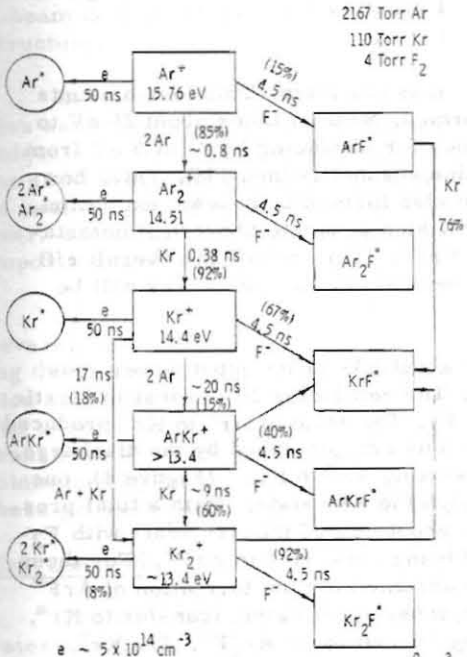

Figure 3. Ion Channels for KrF^* Formation

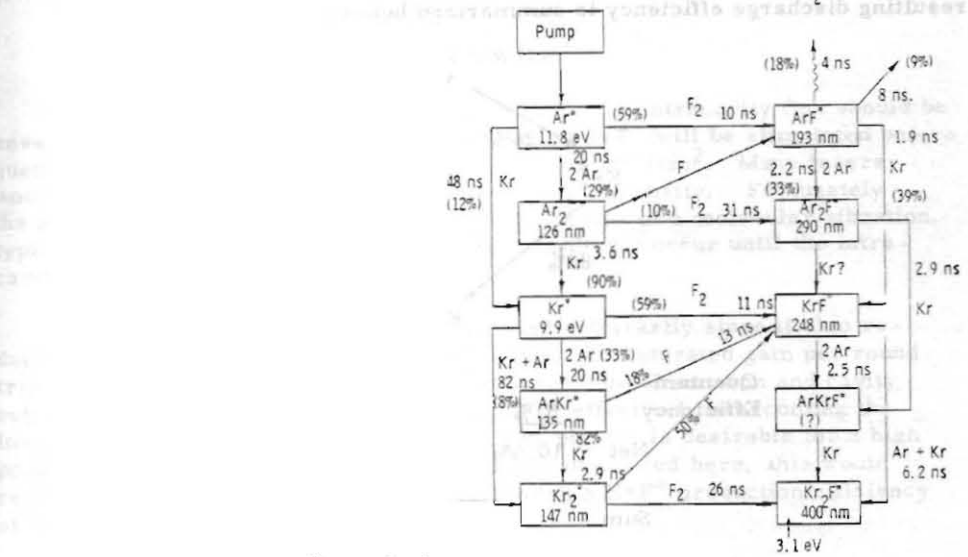

Figure 4. Neutral Channels for KrF^* Formation

These reactions are responsible for populating the KrF^* and ArF^* states. Some of the ArF^*, which is formed in the recombination of Ar^+ and Ar_2^+, is converted to KrF^* through the replacement reaction,

$$ArF^* + Kr \rightarrow KrF^* + Ar$$

The rest is lost via quenching and spontaneous emission. This loss amounts to about 10% of the Ar^+ ions originally formed. Since it takes about 26 eV to create each Ar^+ ion, the quantum efficiency for producing KrF^* at 5 eV from Ar^+ is 19%, and the net efficiency of the ion channel is then 17%. This, however, neglects the metastables which are also formed by e-beam excitation. The same 26 eV which produce one ion will also generate about 0.3 metastables which have a 63% chance of forming KrF^*. This raises the overall efficiency for e-beam pumping to 20%. The neutral channel processes will be discussed below.

Under discharge excitation of KrF, about 80% of the input power goes into excited rare gas states Ar^* and Kr^*. The remaining 20% is lost in elastic scattering and dissociative attachment to F_2. The ratio of Ar^* to Kr^* produced is about two to one (see below). Very few ions are generated by the discharge. There are two dominant channels for converting Ar^* to KrF^* (Figure 4), one through the ArF^* state and the other through the Kr^* state. With a total pressure of three atmospheres and 0.17% F_2, about 60% of the Ar^* react with F_2 to form ArF^*, which has a 55% chance of being converted to KrF^*. For these estimates, a 100% branching ratio [17] is assumed for the formation of ArF^* and KrF^* from F_2. About 37% of the Ar^* undergo excitation transfer to Kr^*, either directly or via Ar_2^*. The remaining 3% end up as Ar_2F^*. The Kr^*, formed either through this channel or directly by the discharge, have a 60% chance of producing KrF^*. The other 40% go into forming the rare gas dimers $ArKr^*$ and Kr_2^*. It is believed that when these excited states react with F_2 about half of them produce KrF^* and the rest form the $ArKrF^*$ states. The resulting discharge efficiency is summarized below:

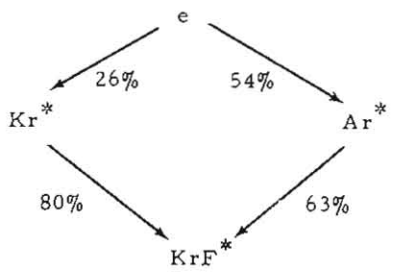

Quantum Efficiency	51%	42%
Net	10.6%	14.3%
Sum	25%	

Discharge pumping of KrF^* is slightly more efficient than pure e-beam pumping based on energy deposited. However, wall-plug efficiency for the e-beam device will be much less due to losses in the foil and foil support structure.

In summary, both electron beam and discharge pumping lead to efficiencies as high as 20-25% for the formation of KrF^*. This is the result of a unique combination of the high efficiency of energy deposition in rare gases, the 100% branching ratio for the formation of KrF^*, the high quantum efficiency, as well as the high rate of intermediate step reactions to form KrF^*. However, achieving this high efficiency in KrF lasers depends upon solving two important problems.

First, in addition to a high rate of spontaneous emission, KrF^* gets severely quenched by various species. This can be counteracted by increasing the intracavity flux to provide a sufficiently high rate of stimulated emission such that KrF^* lases before it gets quenched. The second problem arises due to some intrinsic medium absorption caused by transient species. This transient absorption lowers the cavity extraction efficiency. Its effect can be minimized by having a higher ratio of small signal gain to absorption. Both of these problems and their possible solutions are discussed below in more detail.

KrF Quenching

The various species responsible for quenching KrF^* along with their rates are shown in Table 2 for a mixture of 2167 Torr Ar with 110 Torr Kr and 4 Torr F_2. The decay rate k of KrF^* is found to be 5.6×10^8/sec. The rate of stimulated emission is given by $\frac{I\sigma}{h\nu}$, where I is the intracavity flux. The flux at which the stimulated emission rate equals the quenching rate is given by

$$I_s = \frac{h\nu}{\sigma} k$$
$$= 2.24 \text{ MW/cm}^2$$

In order to prevent the effect of quenching, the intracavity flux should be several times larger than I_s. Eighty percent of KrF^* will be stimulated before quenching if the intracavity flux is 4 I_s, i.e., ~ 9 MW/cm^2. Many lasers would bottleneck at the terminal state at this high intensity. Fortunately the KrF ground state dissociates in the time period of a molecular vibration, typically 10^{-13} sec; therefore bottlenecking would not occur until the intracavity flux becomes $\sim 4 \times 10^{10}$ W/cm^2.

The intracavity flux cannot be increased arbitrarily since it also reduces the gain coefficient. At the steady state, the saturated gain per round trip has to equal the combined losses due to medium absorption and cavity output coupling. To provide sufficient gain for effectively overcoming the losses, a small-signal gain coefficient of 10% per cm is desirable for a high power KrF laser. For the particular mixture discussed here, this would require a pump power of ~ 1 MW/cm^3 assuming a KrF^* production efficiency of 20%.

Table 2.

The process and their rates of quenching KrF^* in a mixture of $Ar/Kr/F_2$ = 2167/110/4

Process			Rate Coefficient	Rate/Sec
$KrF^* + 2Ar$	⟶	$ArKrF^* + Ar$	5×10^{-32} cm^6	2.5×10^8
$KrF^* + Kr + Ar$	⟶	$Kr_2F^* + Ar$	4.7×10^{-31} cm^6	1.2×10^8
$KrF^* + F_2$	⟶	Products	6×10^{-10} cm^3	0.8×10^8
KrF^*	⟶	$Kr + F + h\nu$	9×10^{-9} sec	1.1×10^8
			Total	5.6×10^8

Medium Absorption

The dominant absorbing species and their cross sections in a KrF laser are shown in Table 3.

Table 3. Dominant Absorbing Species in a KrF Laser Media

Absorbing Species	Cross Section (cm^2) at 250 nm
Ar_2^+	1.5×10^{-17}
Kr_2^+	1.5×10^{-18}
F^-	5.6×10^{-18}
F_2	1.5×10^{-20}

There is some additional absorption due to Kr_2F^* which can be neglected at high rates of stimulated emission since formation of Kr_2F^* would then be prevented. Except for F_2, the number density of transient species must be calculated by detailed computer modeling to determine the net absorption coefficient. The computed values agree fairly well [18] with the measured values shown in Figure 5. The measured coefficient for the mixture discussed here was ~1%/cm at a pump power of 1 MW/cm . This absorption severely restricts the cavity extraction efficiency, η_c. η_e is defined as the ratio of

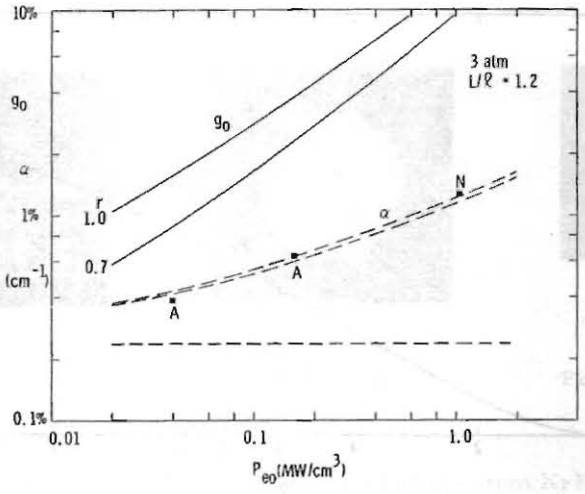

Figure 5. Small-Signal Gain (g_o) and Absorption (a) (e-beam + discharge)

actual output intensity to the intensity which would be obtained if every KrF* generated in the cavity resulted in a photon leaving the output mirror. For a distributed medium absorption coefficient α, the cavity extraction efficiency is given [18] by

$$\eta_c = \frac{1}{2L}\left(\ell n \frac{1}{R}\right)\left(\frac{1}{\alpha + \frac{1}{2L}\ell n \frac{1}{R}} - \frac{1}{g_o}\right)$$

where L = Laser length
R = Reflectivity of the output coupler
g_o = Small signal gain coefficient.

The optimum reflectivity can be obtained from the above expression to be

$$\frac{1}{2L}\ell n\left(\frac{1}{R}\right) = \sqrt{\alpha g_o} - \alpha$$

and therefore the maximum extraction efficiency is

$$\eta_c^{max} \sim \left(1 - \sqrt{\frac{\alpha}{g_o}}\right)^2$$

This function is plotted in Figure 6. For the chosen gas mixture and pressure, $g_o/\alpha \sim 10$ (see Figure 5) at a pump power of 1 MW/cm^3 and therefore the maximum cavity extraction efficiency for this case will be 50%, leading to an intrinsic e-beam pumped laser efficiency of 10% and discharge pumped laser efficiency of ~12%.

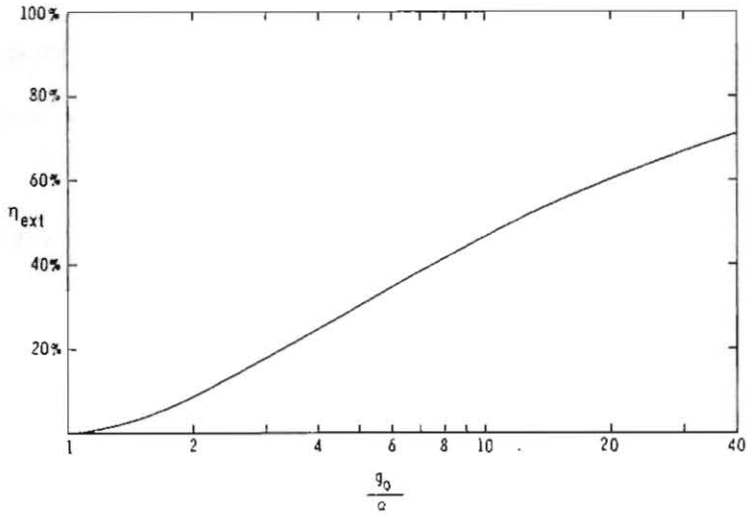

Figure 6. Laser Extraction Efficiency

Results of Small Scale Laser Experiments

The best results obtained so far with a small laser pumped by e-beam alone were from a device shown in Figure 7. The details of this device, using a coaxial e-beam diode were described earlier [19]. The optical cavity in these experiments was formed by two output couplers of 50% and 70% reflectivity, placed at opposite ends of the 20 cm gain length. The laser pulse width from KrF (Figure 8) was typically 125 ns, which closely corresponded to the e-beam pulse width.

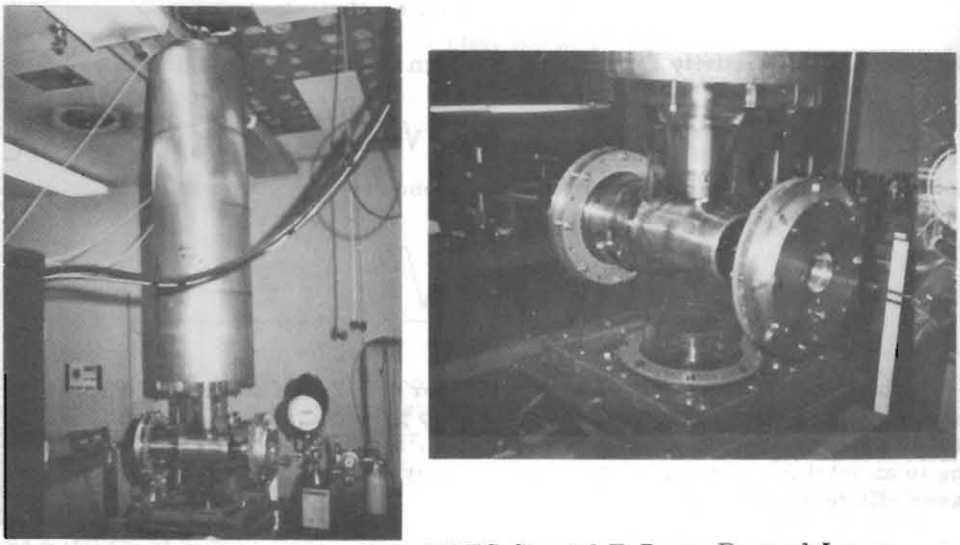

Figure 7. Photographs of the NRTC Coaxial E-Beam Pumped Laser

(a) (b) (c)

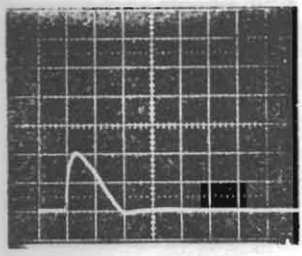

100 ns/div
10 V/div
F4115 Photodiode

Burn Pattern
≈ 1.5 J

Focused Burn
Pattern
≈ 1.5 J

Figure 8. Photodiode Trace and Burn Patterns from KrF

The largest energy extracted from KrF was 3.3 J from a 3 atm mixture containing 0.3% F_2, 4.7% Kr, and 95% Ar. The energy deposition into the gas was estimated to be 28 J from the pressure rise inside the anode, as determined from the measured strength of the compression wave leaving the excitation region. Thus an intrinsic laser efficiency of 11.9% was obtained with a pump power of ~20 MW/cm^3. This agrees fairly well with the theoretical expectations discussed earlier.

The laser burn pattern presented in Figure 8 indicates that the active volume was close to the geometrical value of 0.101 liters. Thus under optimum conditions, the laser was operating with an output of 33 J/ℓ with an intrinsic efficiency of 12%.

Comparable results were also obtained [20] by e-beam controlled discharge pumping using the device shown in Figure 9. A schematic of the apparatus is shown in Figure 10. The cold cathode electron gun had a 22 cm x 4 cm aperture. A supported 1 mil titanium foil acted as the anode. The e-gun foil formed the positive discharge electrode while a modified Rogowski-profiled aluminum bar formed the discharge cathode. Energy stored in the discharge capacitor was switched on to the cathode at the same instant that the e-gun was energized.

The discharge capacitor was 0.225 μJ and could be charged up to 30 kV, for a stored energy of 101 J. The circuit inductance was measured to be 160 nH. The optical cavity was formed by a partial reflector (77%) and a total reflector (98%), mounted 50 cm apart on the ends of the laser plenum.

The highest output energy of 3.2 J from KrF* was achieved with a gas mixture containing 0.14% F_2, 4.5% Kr, and 95.4% Ar at a total pressure of 3 atm. The output waveforms are shown in Figure 11. The e-beam current density under these conditions was checked before and after the laser shot and indicated 40 A/cm^2 with a pulselength of 220 ns. The maximum discharge voltage and current were 4.5 kV and 20 kA, respectively. The 3.2 J output came in a pulse 160 ns wide (FWHM), for an average power of 20 MW. The

Figure 9. E-Beam Sustained Discharge Laser

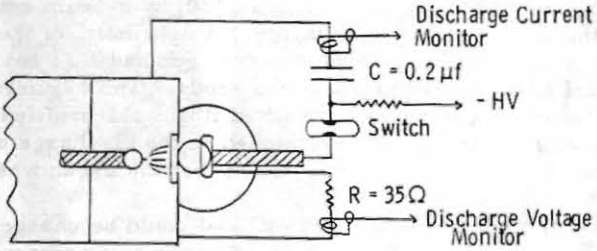

Marx Voltage	300 kV
J_B	5 - 40 A/cm^2
Pulselength	250 ns
Extracted Volume	100 - 200 cm^3

Figure 10. Discharge Circuit and Diagnostics

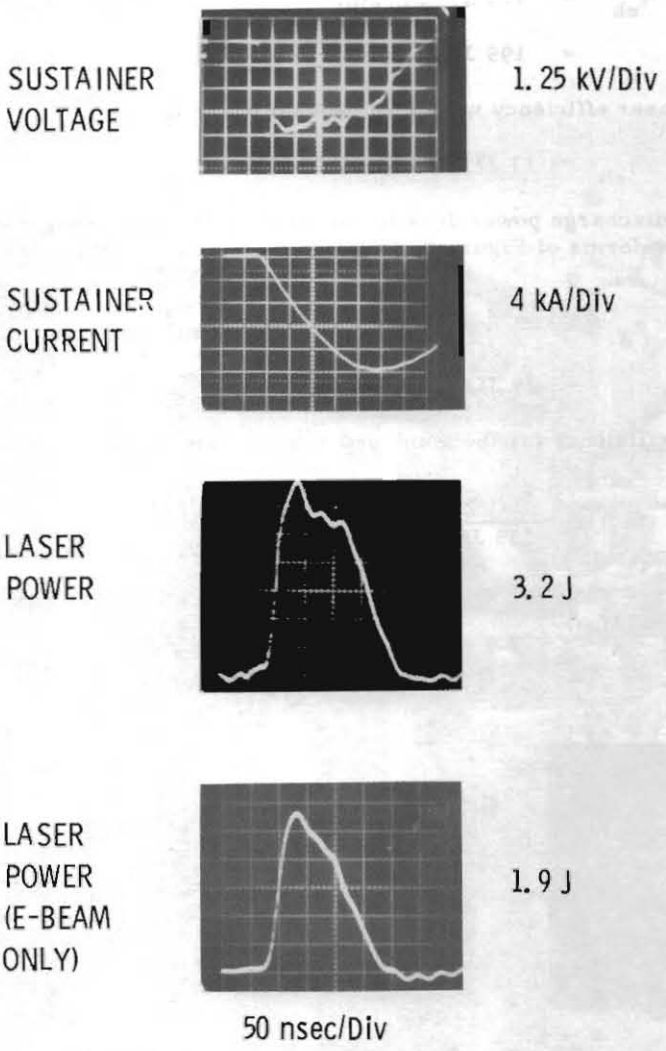

Figure 11. Waveforms for Highest Energy Output from a Small Laser Using E-Beam Controlled Discharge Pumping

burn pattern, shown in Figure 12, indicates an extracted area of 5.6 cm^2. Since the output coupler was an 80% reflector, the intracavity intensity must have been 18 MW/cm^2 or about eight times the saturation intensity. The specific energy extracted from a volume of 112 cm^3 was 29 J/ℓ.

Under the same conditions as above, the e-beam alone gave 1.9 J laser output for a specific energy of 17 J/ℓ. The stopping power of the laser gas was 7.4 kV/cm/atm (including a factor of 3 to account for the effects of electron scattering) which gives a deposited energy of

$$\mathcal{E}_{eb} = 7.4\ \text{kV/cm/atm} \cdot 3\ \text{atm} \cdot 40\ \text{A/cm}^2 \cdot 220\ \text{ns}$$

$$= 195\ \text{J/}\ell$$

Thus the laser efficiency with pure e-beam pumping was

$$\eta_{eb} = 17\ \text{J/}\ell / 195\ \text{J/}\ell = 9\%$$

The discharge power density can be found by integrating under the current-voltage waveforms of Figure 11 up to the termination of the laser pulse. This gives

$$\mathcal{E}_d = \frac{2}{\pi} \cdot 2.25\ \text{kV/cm} \cdot 250\ \text{A/cm}^2 \cdot 220\ \text{ns}$$

$$= 79\ \text{J/}\ell$$

The laser efficiency for the combined e-beam plus discharge pumping was therefore,

$$\eta = \frac{29\ \text{J/}\ell}{195\ \text{J/}\ell + 79\ \text{J/}\ell} = 11\%$$

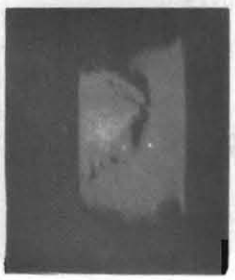

BURN PATTERN

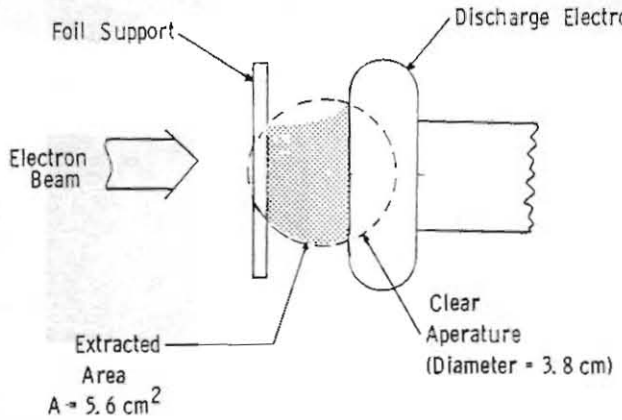

Volume = 20 cm x 5.6 cm² = 112 cm³

Figure 12. Extracted Volume from NRTC 0.1 Liter Device

Results of Large Scale Experiments

Several large scale devices have been built to investigate the volume scalability of the rare gas halide lasers by both e-beam and e-beam sustained discharge pumping. A photograph of the Northrop device is shown in Figure 13. The results of Northrop [21], Avco [22], and Maxwell Laboratories [23] devices

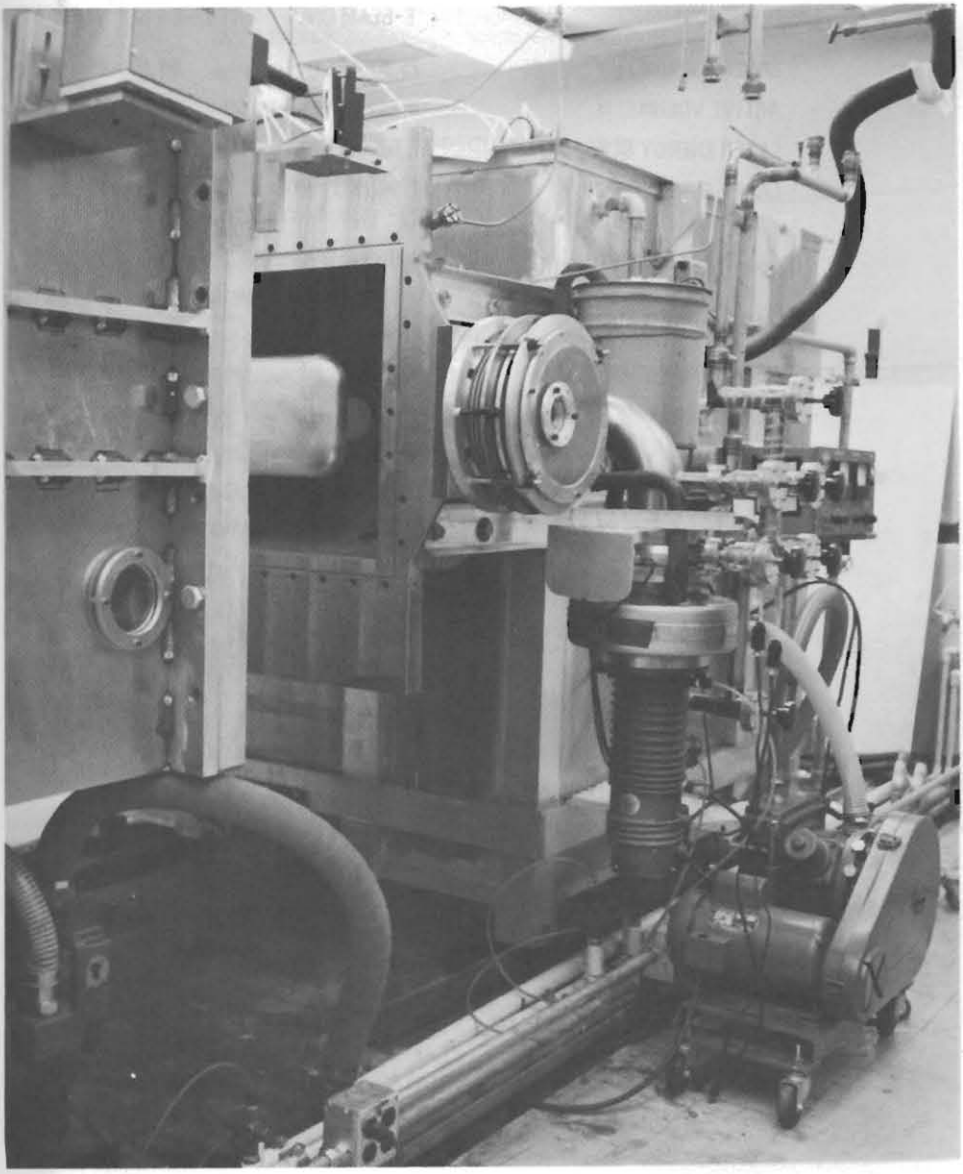

Figure 13. Northrop's 10 Liter KrF Laser Pumped by E-Beam Sustained Discharge

Table 4. Northrop Results

	E-BEAM ONLY	DISCHARGE ADDED E/N~2 x 10^{-17} Vcm^2
• LASER PERFORMANCE		
- LASER ENERGY	75 JOULES	90 JOULES
- ACTIVE VOLUME	10 LITERS	10 LITERS
- LASER ENERGY DENSITY	7.5 J/LITER	9 J/LITER
- LASER ENERGY/ENERGY DEPOSITED	7.5% (7.5 / 100)	7.5% (9 / 120)
- LASER PULSE LENGTH	900 nsec	
• E-BEAM CHARACTERISTICS		
- BEAM CURRENT DENSITY	10 - 18 A/cm^2	
- BEAM ENERGY	320 keV	
• LASER GAS MIXTURE		
- 0.14% F_2 / 7.2% Kr / 92.66% Ar at 1.7 atm		

Table 5. Avco Results (E-Beam Only)

• LASER PERFORMANCE	
- LASER ENERGY	= 102 JOULES
- ACTIVE VOLUME	= 8.5 LITERS
- LASER ENERGY DENSITY	= 12 J/LITER
- LASER ENERGY/ENERGY DEPOSITED	= 9%
- LASER PULSE LENGTH	= 600 nsec
• E-BEAM CHARACTERISTICS	
- BEAM CURRENT DENSITY	= 11.5 A/cm^2
- BEAM ENERGY	= 250 keV
• LASER GAS MIXTURE	
- 0.2% F_2 / 4% Kr / 95.8% Ar at 1.7 atm	

Table 6. Avco Results (Discharge Added)

- LASER PERFORMANCE
  - LASER ENERGY = 75 JOULES
  - ACTIVE VOLUME = 7.5 LITERS
  - LASER ENERGY DENSITY = 10 J/LITER
  - LASER ENERGY/ENERGY DEPOSITED = 9.5%
  - LASER PULSE LENGTH = 500 nsec
  - OUTPUT COUPLING = 71%
- DISCHARGE CHARACTERISTICS
  - DISCHARGE ELECTRIC FIELD = 2 kV/cm-atm
  - DISCHARGE CURRENT DENSITY = 70 A/cm^2
  - DISCHARGE ENERGY DEPOSITED = 70 J/LITER
- E-BEAM CHARACTERISTICS
  - BEAM CURRENT DENSITY = 4 A/cm^2
  - BEAM ENERGY = 300 keV
  - BEAM ENERGY DEPOSITED = 35 J/LITER
- LASER GAS MIXTURE
  - 0.5% F_2 / 10% Kr / 89.5% Ar at 1.5 atm

Table 7. Maxwell Lab Results

- LASER PERFORMANCE
  - LASER ENERGY = 350 JOULES
  - ACTIVE VOLUME = 60 LITERS (200 x 20 x 15 cm)
  - LASER ENERGY DENSITY = 5.8 J/LITER
  - LASER ENERGY/ENERGY DEPOSITED = $10\% \left(\frac{350}{3.5 \times 10^3} \right)$
- E-BEAM CHARACTERISTICS
  - BEAM CURRENT DENSITY = $< 10\ A/cm^2$
  - BEAM ENERGY = ~250 keV
- LASER GAS MIXTURE
  - 0.1% F_2 / 7% Kr / 92.9% Ar at 1 atm

are summarized in Tables 4, 5, 6 and 7. These results clearly indicate the volume scalability of e-beam pumping. Efficient discharge pumping in these devices was hampered by discharge instability resulting from a non-uniform e-beam deposition. A detailed analysis shows [18] that efficient e-beam stabilized discharge pumping should be possible if a uniform e-beam deposition is achieved by using two opposed e-beams.

FLUID DYANMICS OF UV VISIBLE LASERS

The high pump power requirements for efficient operation of the excimer lasers exclude the possibility of a cw laser of this type. Therefore, the only way a high average power can be achieved is by repetitive pulsing of the laser. This obviously requires gas flow through the cavity for heat rejection. Due to the high pressure requirements of the excimer laser, a supersonic flow would be impractical. For a subsonic flow, a Mach number of 0.3-0.4 is desirable in order to avoid excessive turbulence. A conceptual design of such a laser using e-beam pumping is shown in Figure 14. Discharge excitation may be added as in the case of single pulse operation.

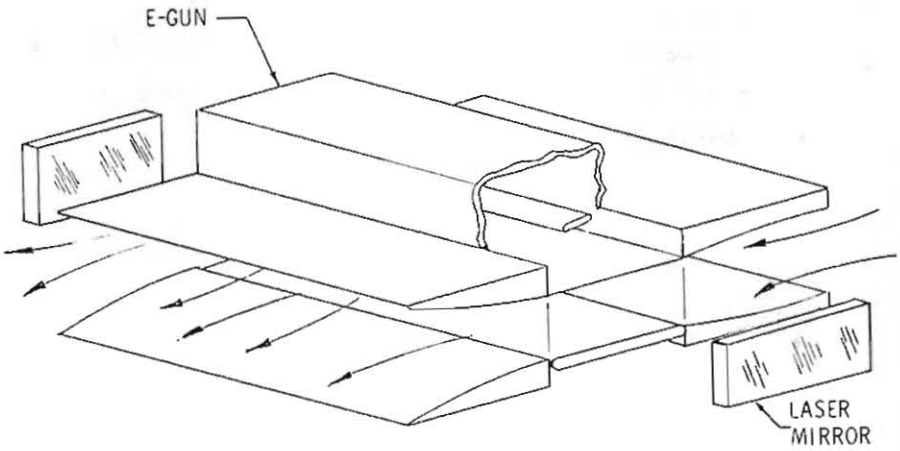

Figure 14. Schematic of a Repetitively Pulsed Excimer Laser

A repetitively pulsed laser of the above design requires a very uniform medium density to obtain a good beam quality. The combination of high gas density and the short laser wavelength requires nearly two orders of magnitude better medium homogeneity than that required for high average power CO_2 lasers. Furthermore, the pressure wave generated by the pump pulse will create shock waves which must be damped out in between the laser pulses. Also, nonuniformity in energy deposition within the cavity will cause

additional disturbances. In general, to obtain a good beam quality, these disturbances must be "flushed" downstream even after adequate damping. This requires a cavity gas flush factor of nearly 1.5. The medium homogeneity and acoustic damping requirements are discussed below for a laser pressure of 2.5 atm using Ar as a diluent.

Permissible Density Disturbance

Propagation of a laser beam through a turbulent gain medium of length L causes an attenuation in the center of the far-field, given by

$$\frac{I}{I_o} = e^{-\alpha L}$$

where the attenuation coefficient α can be expressed in terms of a fluctuation in the refractive index n [24]:

$$\alpha = 2\left(\frac{2\pi}{\lambda}\right)^2 \langle \Delta n^2 \rangle s ,$$

where s is the scale length of the turbulent eddies.

Alternatively, the permissible fluctuation in the refractive index squared for a given maximum far-field attenuation is

$$\langle \Delta n^2 \rangle = \frac{\alpha}{2s}\left(\frac{\lambda}{2\pi}\right)^2 .$$

Substituting for α this becomes

$$\langle \Delta n^2 \rangle = \frac{1}{2Ls}\left(\frac{\lambda}{2\pi}\right)^2 \ell n \frac{I_o}{I}$$

If we approximate the statistical root-mean-square value with a simple average change in n, we can write:

$$\Delta n \approx \sqrt{\langle \Delta n^2 \rangle} = \frac{\lambda}{2\pi}\sqrt{\frac{\ell n\,(I_o/I)}{2\,sL}}$$

But $$\frac{\Delta n}{n-1} = \frac{\Delta}{\rho} \quad \text{since } n = 1 + \beta\frac{}{\rho_s}$$

(where β is Gladstone-Dale constant). Therefore, the permissible density fluctuation becomes

$$\frac{\Delta\rho}{\rho} = \frac{\lambda}{2\pi}\,\frac{1}{(n-1)}\sqrt{\frac{\ell n\,(I_o/1)}{2sL}}$$

and the corresponding pressure fluctuations are given by

$$\frac{\Delta p}{p} = \gamma\,\frac{\Delta\rho}{\rho}$$

where the pressure amplitude has been assumed to be sufficiently small, so that the isentropic relation $p = \rho^{\gamma}$ applies.

Application to E-Beam Pumped KrF Laser

For a typical KrF laser the following conditions may be taken as representative:

Gas pressure: 2.5 atm (essentially all argon);
(This gives a value of $n - 1 = \beta / f_s = 7.025 \times 10^{-4}$)

Gain length: $L = 1$ m

Turbulence scale: $s = 3$ mm

Laser Wavelength: $\lambda = 249$ nm

We will require that the far-field beam attenuation due to turbulence in the gain medium is no more than 20%. This makes $\ell n\,(I_o/I) = 0.223$. To satisfy this condition $\Delta\rho/\rho$ for the undisturbed medium has to be 3.4×10^{-4}.

The most severe acoustic disturbance in the laser medium is the shock wave produced by the sudden energy addition to the laser medium by the pump pulse. The initial heat content of the monatomic laser gas at 2.5 atm and 300°K is 0.38 J/cm^3. A pumping pulse of 1 MW/cm^3, lasting half a microsecond, adds approximately the same amount of energy again, assuming 75% of the energy goes into gas heating. This causes an immediate doubling of the temperature and pressure

$$T_4/T_1 = p_4/p_1 = 2.0$$

or

$$\Delta T/T = \Delta p/p = 1.0$$

whereas the density remains approximately constant due to the inertia of the gas and the short duration of the pumping pulse. After the laser pulse, shock waves will generate severe density disturbances. The waves generated by a laser pump pulse are generally three-dimensional. However, in an idealized form, one can visualize a pair of one-dimensional compression waves propagating outward from the discharge region while rarefaction fans propagate into the discharge region.

The strength, M_s, of the shock wave generated can be estimated from the one-dimensional shock tube relation using p_4/p_1 as the diaphragm pressure ratio:

$$\frac{p_4}{p_1} = \left(\frac{\gamma-1}{\gamma+1}\right)\left(\frac{2\gamma}{\gamma-1}\,M_s^{\,2} - 1\right)\left[1 - \frac{(\gamma-1)\,(M_s^{\,2}-1)}{(\gamma+1)\,(T_4/T_1)^{1/2}\,M_s}\right]^{-\frac{2\gamma}{\gamma-1}}.$$

For the special case of $T_4/T_1 = 2$ and $\gamma = 5/3$ (monatomic gas) this equation becomes:

$$\frac{p_4}{p_1} = \frac{1}{4}\left(5\,M_s^2 - 1\right)\left(1 - \frac{M_s^2 - 1}{5.657\,M_s}\right)^{-5}$$

Solving for M_s and substituting $p_4/p_1 = 2.00$ gives $M_s = 1.178$ for the shock Mach number.

The pressure ratio p_2/p_1 across a normal shock is given by:

$$\frac{p_2}{p_1} = \frac{2\gamma}{\gamma+1}\left(M_s^2 - \frac{\gamma-1}{2\gamma}\right)$$

$$= 1.25\left(M_s^2 - 0.2\right) \text{ for } \gamma = 5/3.$$

Hence, $p_2/p_1 = 1.485$, or $(\Delta p/p)_{SHOCK} = 0.485$. But the maximum permissible pressure fluctuation $(\Delta p/p)_{PERM}$ is given by

$$(\Delta p/p)_{PERM} = 5.73 \times 10^{-4}$$

The pressure amplitude, therefore, has to be attenuated by acoustic damping techniques by a factor of

$$\frac{(\Delta p)_{PERM}}{(\Delta p)_{SHOCK}} = 1.18 \times 10^{-3}$$

In units of decibels, this corresponds to

$$20 \log_{10} \frac{(\Delta p)_{PERM}}{(\Delta p)_{SHOCK}} = -58.6 \text{ dB}$$

Both upstream and downstream shock absorbers must be designed to provide such attenuations. These attenuators must also be compatible with thermal gas conditioners to give an undisturbed flow homogeneity of $\Delta\rho/\rho \sim 10^{-4}$.

In conclusion, the development of high average power uv visible lasers requires solution to some difficult fluid dynamic problems. So far, adequate attention has not been focused on these problems, although their solution is essential for a practical high power uv visible laser required for many important applications.

REFERENCES

1. N. G. Basov, V. A. Danilychev, and Y. M. Popov, Sov. J. Quantum Electron. 1, 18 (1971); H. A. Koehler, L. J. Ferderber, D. L. Readhead, and

P. J. Ebert, Appl. Phys. Lett. 21, 198 (1972); P. W. Hoff, J. C. Swingle, and C. K. Rhodes, Opt. Commun. 8, 128 (1973); E. R. Ault, M. L. Bhaumik, W. M. Hughes, R. J. Jensen, C. P. Robinson, A. C. Kolb and J. Shannon, IEEE J. Quantum Electron. 9, 1031 (1973).

2. E. R. Ault, M. L. Bhaumik, and N. T. Olson, IEEE J. Quantum Electron. 10, 624 (1974); S. K. Searles and G. A. Hart, Appl. Phys. Lett. 25, 79 (1974).

3. J. E. Velazco and D. W. Setser, J. Chem. Phys. 62, 1990 (1975).

4. C. A. Brau and J. J. Ewing, Appl. Phys. Lett. 27, 435 (1975).

5. E. R. Ault, R. S. Bradford, Jr., and M. L. Bhaumik, Appl. Phys. Lett. 27, 413 (1975).

6. J. J. Ewing and C. A. Brau, Appl. Phys. Lett. 27, 350 (1975).

7. S. K. Searles and G. A. Hart, Appl. Phys. Lett. 27, 243 (1975).

8. R. S. Bradford, Jr., E. R. Ault, and M. L. Bhaumik, Electronic Transition Lasers, ed. J. I. Steinfeld (M. I. T. Press, Cambridge, 1975), p. 211.

9. R.S. Bradford, Jr., E. R. Ault, and M. L. Bhaumik, Appl. Phys. Lett. 27, 546 (1975).

10. J. J. Ewing and C. A. Brau, Appl. Phys. Lett. 27, 557 (1975).

11. M. L. Bhaumik, R. S. Bradford, Jr., and E. R. Ault, Appl. Phys. Lett. 28, 23 (1976).

12. T. R. Loree, R. C. Sze and D. L. Barker, Appl. Phys. Lett. 31, 37 (1977).

13. J. H. Parks, Appl. Phys. Lett. 31, 192 (1977).

14. P. J. Hay and T. H. Dunning, Jr., J. Chem. Phys. 66, 1306 (1977).

15. J. Tellinghuisen, A. K. Hays, J. M. Hoffman, and G. C. Tisone, J. Chem. Phys. 65, 4473 (1976).

16. G. P. Quigley and W. M. Hughes, Appl. Phys. Lett. 32, 627 (1978).

17. J. E. Velazco, J. H. Kolts, and D. W. Setser, J. Chem. Phys. 65, 3468 (1976).

18. W. H. Long, Jr., R. S. Bradford, Jr., J. B. West, and M. L. Bhaumik, "UV Gas Laser Investigations," Northrop Report NRTC 77-15R.

19. E. R. Ault, Appl. Phys. Lett. 26, 619 (1975).

20. R. S. Bradford, Jr., W. B. Lacina, E. R. Ault, and M. L. Bhaumik, Opt. Commun. 18, 210 (1976).

21. D. B. Cohn and W. B. Lacina, "High Power Short Wavelength Laser Development," Northrop Report NRTC 77-43R.

22. M. Rokni, J. A. Mangano, J. H. Jacob and J. C. Hsia, IEEE J. Quantum Electron. 14, 464 (1978)

23. R. Hunter, 7th Winter Colloquium on High Power Visible Lasers, Park City, Utah, February 16-18 (1977).

24. G. W. Sutton, AIAA J. 7, 1737 (1969).